Electronic Supplementary Material (ESI) for Nanoscale Advances.

Supplementary Information

Optimization of $CoFe_2O_4$ Nanoparticles and Graphite Fillers to Provide Thermoplastic Polyurethane Nanocomposites with Superior Electromagnetic Interference Shielding Performance

Anju, Milan Masař, Michal Machovský, Michal Urbánek, Pavol Šuly, Barbora Hanulíková, Jarmila Vilčáková, Ivo Kuřitka, Raghvendra Singh Yadav*

Centre of Polymer Systems, University Institute, Tomas Bata University in Zlín, Trida Tomase Bati 5678, 760 01 Zlín, Czech Republic

*Corresponding author: Raghvendra Singh Yadav, Email: yadav@utb.cz

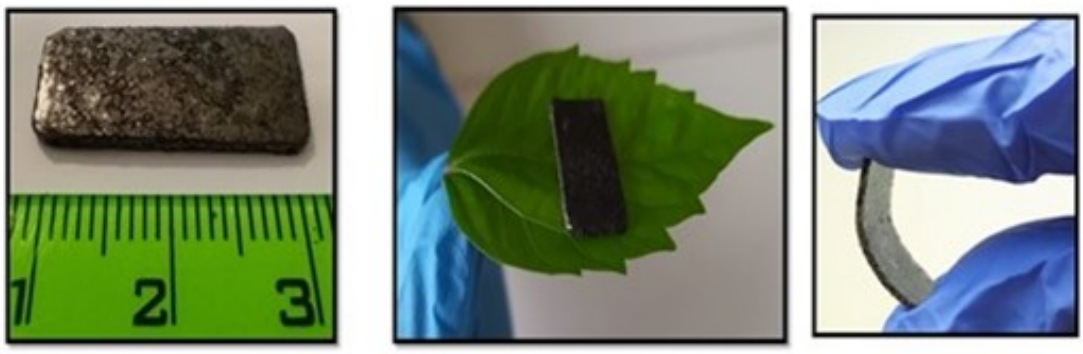

Fig. S1: Digital photograph showing dimensions, light-weight, and flexibility of the developed nanocomposite.

Raman and FTIR spectroscopy:

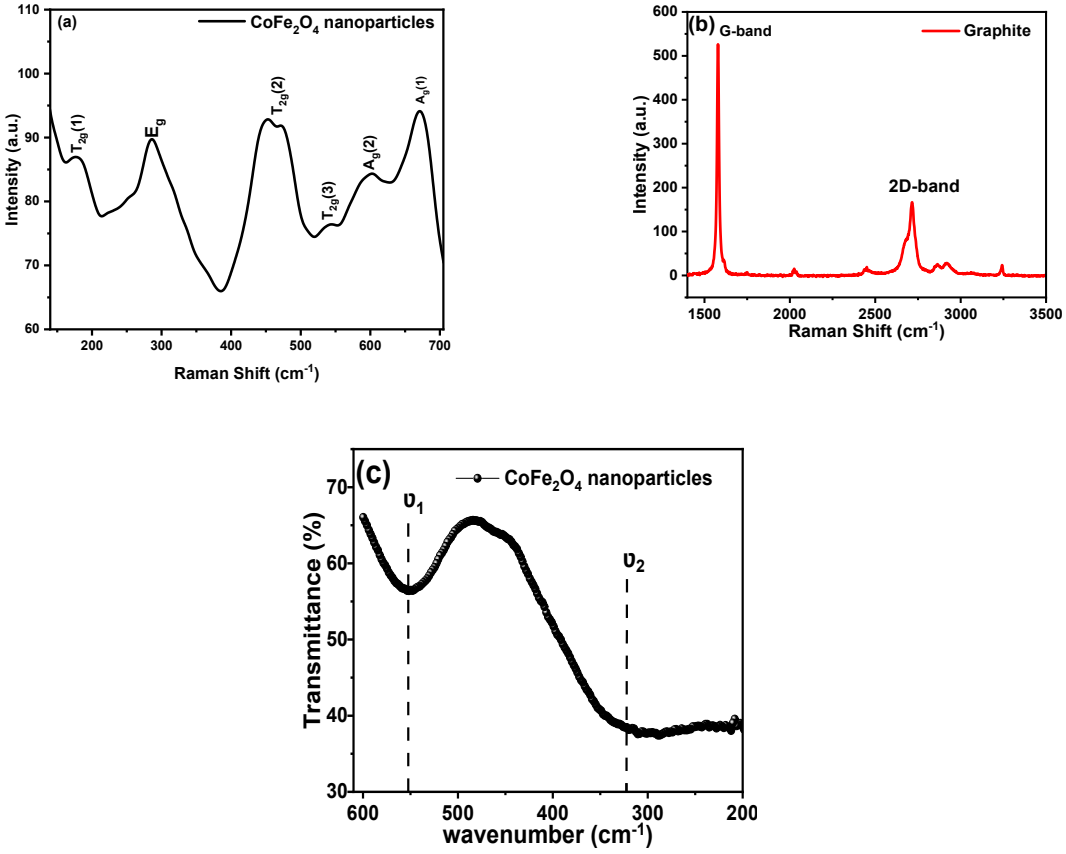

Fig. S2: (a) Raman spectrum of $CoFe_2O_4$ nanoparticles **(b)** Raman spectrum of graphite **(c)** FTIR spectrum of $CoFe_2O_4$ nanoparticles.

The Raman spectrum of $CoFe_2O_4$ nanoparticles in **Fig. S2** (a) revealed the presence of all the five Raman modes which are a feature of spinel ferrites structure: 181 cm^{-1}, 284 cm^{-1}, 460 cm^{-1}, 537 cm^{-1}, and 671 cm^{-1} attributed to $T_{2g}(1)$, E_g, $T_{2g}(2)$, $T_{2g}(3)$, and $A_g(1)$ respectively. The existence of $A_g(2)$ at 597 cm^{-1} is a characteristic feature of inverse spinel ferrites [1]. Further, the Raman spectrum of graphite was recorded and illustrated in **Fig. S2 (b)**. As can be seen, the Raman spectra of graphite exhibit two strong Raman active bands at 1580 cm^{-1} and 2712 cm^{-1} attributed to the G-band and 2D band, respectively [2–4]. Further, The FTIR spectrum of $CoFe_2O_4$ nanoparticles is displayed in **Fig. S2 (c)**. As can be seen, the two prominent characteristic frequency bands at 550 cm^{-1} and 330 cm^{-1} are designated to the Fe-O stretching vibrations at the tetrahedral site υ_1 and stretching vibrations of Co-O at the octahedral site, υ_2 respectively [5,6].

4.4 Thermogravimetric Analysis of the Nanocomposites

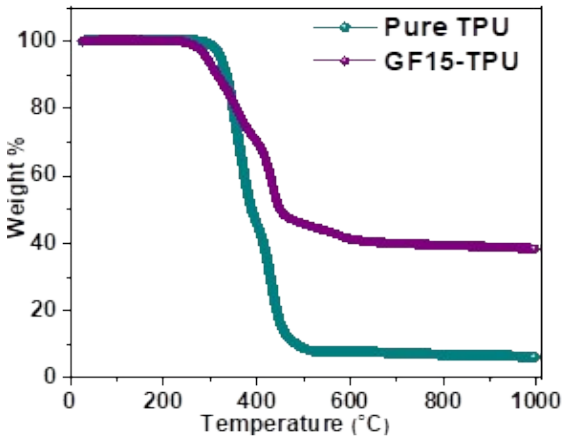

Fig. S3: TGA curves of the developed Pure TPU and GF15-TPU nanocomposites.

Fig S3 demonstrates the TGA curves for the pure TPU and developed GF15-TPU nanocomposite. As can be seen, pure TPU degrades in two stages. The urethane bond of the TPU hard segments decomposes at 285 °C, causing the first stage mass degradation of pure TPU, resulting in the forming of diisocyanate and diol and the following release of CO_2 in the 00°C -350 °C temperature range [7,8]. Further, the second degradation temperature of pure TPU is around 460 °C, which is attributed to the thermal degradation of the soft segments of TPU [9]. In the case of the developed GF15-TPU nanocomposite, thermal degradation occurred in three stages. The initial degradation temperature for GF15-TPU was reduced to 242 °C. Moreover, the GF15-TPU nanocomposite was monitored to be stable up to 1000 °C, revealing no significant degradation after 600 °C up to 1000 °C. Furthermore, the char residue was significantly higher in the case of developed GF15-TPU nanocomposites than pure TPU owing to the existence of graphite and $CoFe_2O_4$ nanoparticles.

4.5 FE- SEM of GF5-TPU Nanocomposites

Fig S4 (a-b) demonstrates the SEM micrograph of GF5-TPU nanocomposite confirming the presence of graphite, $CoFe_2O_4$ nanoparticles in the TPU matrix. The $CoFe_2O_4$ nanoparticles were observed to slightly agglomerated inside the TPU matrix.

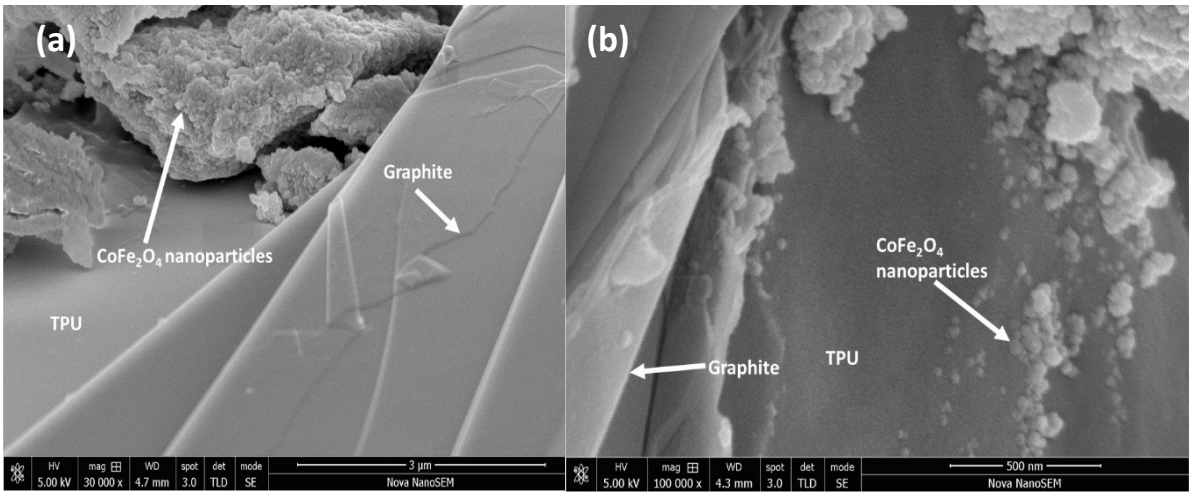

Fig. S4: SEM micrograph of (a) GF5-TPU (b) GF10-TPU nanocomposite.

4.5 EMI shielding effectiveness at thickness 4mm for the developed polymer nanocomposites

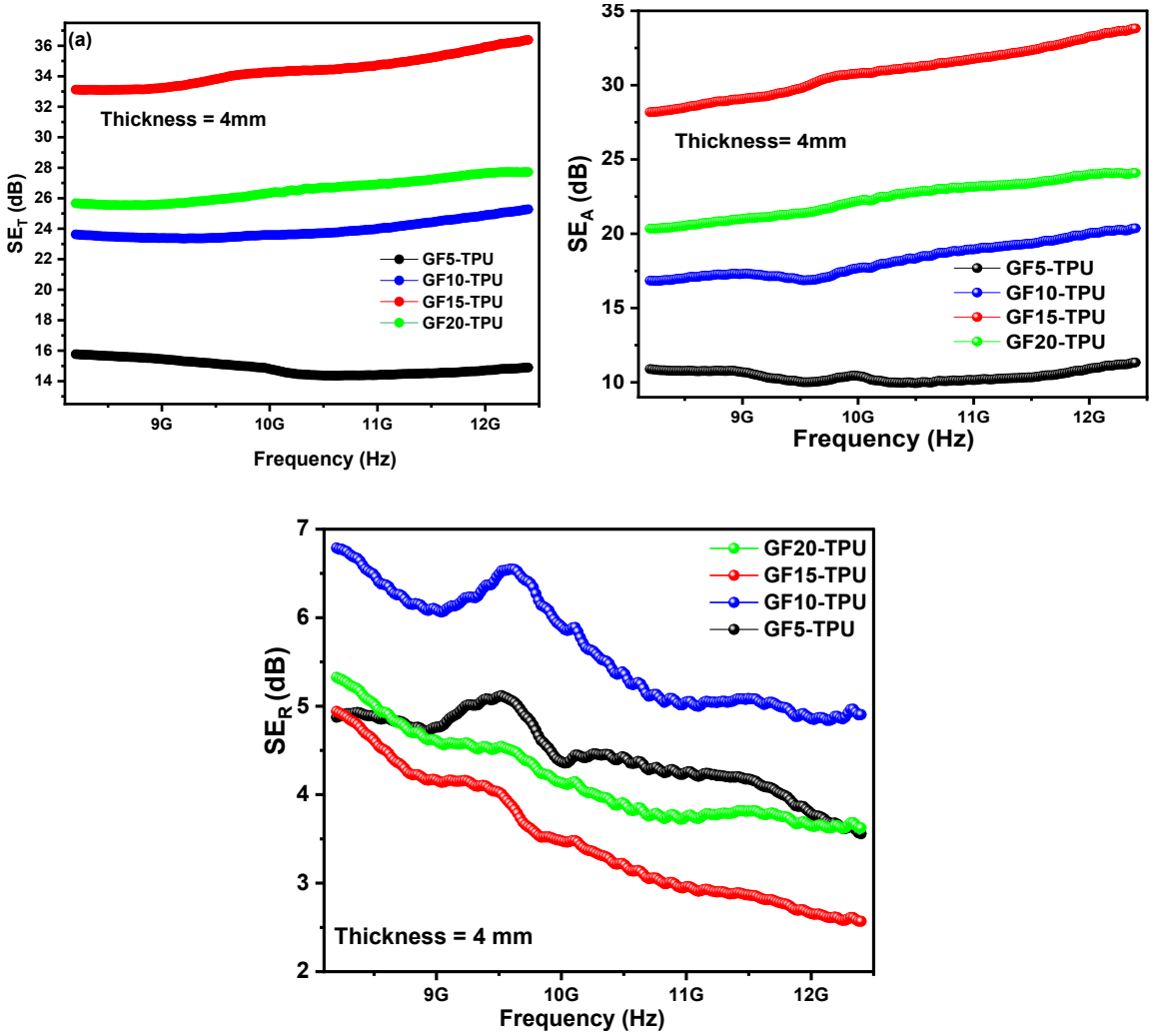

Fig. S5: EMI **(a)** total shielding effectiveness, SE_T **(b)** shielding due to absorption, SE_A **(c)** shielding due to reflection SE_R as a function of frequency in X-band range for the developed nanocomposites with 4 mm thickness.

4.7 Mechanical properties of the Pure TPU and developed nanocomposites

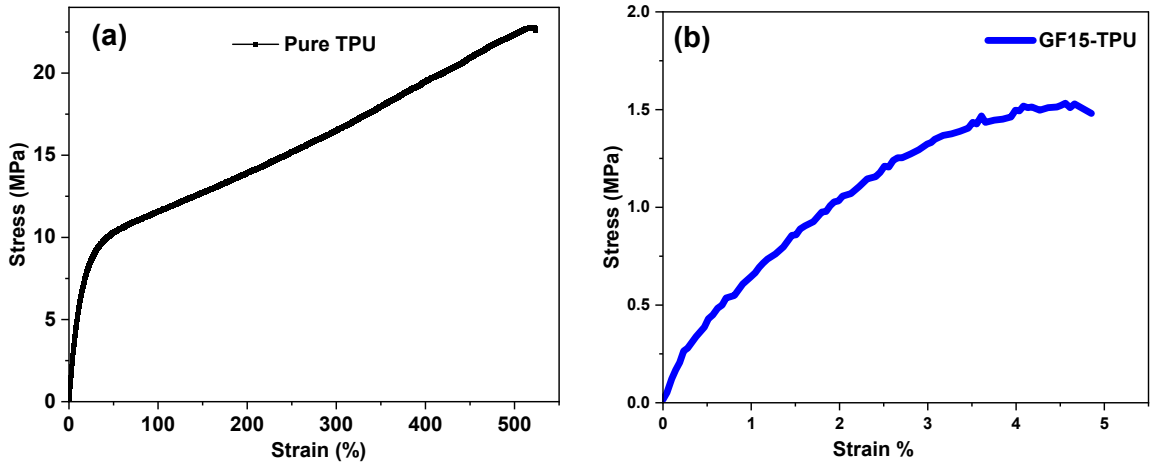

Figure S6: Stress- strain curve for the (a) Pure TPU (b) GF5-TPU and GF15-TPU nanocomposite.

Figure S6 (a-b) demonstrates the representative plots of stress-strain of the Pure TPU and GF15-TPU nanocomposites. The value of Young's modulus was 72.13±5.35 MPa, and 74.09 ± 45.39 MPa for Pure TPU, and GF15-TPU nanocomposite, respectively. A slight improvement in the value of Young's modulus was noticed with introduction of graphite and $CoFe_2O_4$ nanoparticles in the TPU matrix as compared with the pristine TPU. Further, the tensile strength was 24.08±5.91 MPa, and 1.42±0.19 MPa for Pure TPU, and GF15-TPU nanocomposites, respectively [10]. The mechanical characteristics rely on various factors including the filler loading, dispersion and bonding ratio etc. The decrease in the value of the tensile strength can be associated with the high content of filler, which resulted in the decrease in the inter-filler separation distance and therefore decrease in the polymer chains between the fillers. As a result, the fillers which including graphite and $CoFe_2O_4$ nanoparticles are close to each other generating strong filler-filer interactions outspacing the polymer-filler interaction. This can led to the decrease in the load transfer between TPU and the fillers, and therefore reducing the tensile strength of the nanocomposite [10]. Previously Jun et al. [11] also reported a decrease in the value of tensile strength at higher filler loading for graphene nano-ribbon/thermoplastic polyurethane composites.

References:

1 S. M. Ansari, K. C. Ghosh, R. S. Devan, D. Sen, P. U. Sastry, Y. D. Kolekar and C. V. Ramana, *ACS Omega*, 2020, **5**, 19315–19330.

2 A. Kaniyoor and S. Ramaprabhu, *AIP Adv*, , DOI:10.1063/1.4756995.

3 Y. Çelik, E. Flahaut and E. Suvacı, *FlatChem*, 2017, **1**, 74–88.

4 A. C. Ferrari, *Solid State Commun*, 2007, **143**, 47–57.

5 F. A. Sheikh, H. M. N. ul H. Khan Asghar, M. Khalid, Z. A. Gilani, S. M. Ali, N. ul H. Khan, M. A. Shar, H. Mufti and A. Alhazaa, *Physica B Condens Matter*, 2023, **652**, 414656.

6 H. Ghorbani, M. Eshraghi and A. A. Sabouri Dodaran, *Physica B Condens Matter*, 2022, **634**, 413816.

7 H. Li, N. Ning, L. Zhang, Y. Wang, W. Liang and M. Tian, *Polym Degrad Stab*, 2014, **105**, 86–95.

8 K. Chen, H. Wang, Y. Shi, M. Liu, Y. Feng, L. Fu and P. Song, *J Colloid Interface Sci*, 2024, **653**, 634–642.

9 Y. Zhang, J. Cui, L. Wang, H. Liu, B. Yang, J. Guo, B. Mu and L. Tian, *Polym Adv Technol*, 2020, **31**, 1150–1163.

10 J. H. Choe, J. Jeon, M. E. Lee, J. J. Wie, H. J. Jin and Y. S. Yun, *Nanoscale*, 2018, **10**, 2025–2033.

11 Y. seok Jun, S. Habibpour, M. Hamidinejad, M. G. Park, W. Ahn, A. Yu and C. B. Park, *Carbon N Y*, 2021, **174**, 305–316.